J Mater Sci: Mater Electron (2016) 27:5303–5308
DOI 10.1007/s10854-016-4428-2

Synthesis and enhanced luminescent characterization of $SrAl_4O_7:Eu^{2+},RE^{3+}$ (RE = Nd, Dy) nanophosphors for light emitting applications

Devender Singh[1,2] · Vijeta Tanwar[1] · Anura P. Simantilleke[2] · Shri Bhagwan[1] · Bernabe Mari[3] · Pratap Singh Kadyan[1] · Krishan Chander Singh[1] · Ishwar Singh[1]

Received: 29 November 2015 / Accepted: 28 January 2016 / Published online: 3 February 2016

Abstract $SrAl_4O_7:Eu^{2+},RE^{3+}$ (RE = Nd, Dy) nanophosphors were efficiently synthesized with a facile fast gel combustion procedure in presence of air. During the synthesis process, urea was used as an organic fuel. Boric acid was applied as reducer as well as flux for the reduction of Eu^{3+} ions into Eu^{2+}. Phase composition, morphology and photoluminescence (PL) properties of the prepared $SrAl_4O_7:Eu^{2+},RE^{3+}$ phosphors were analyzed by X-ray diffraction, scanning electron microscopy (SEM), transmission electron microscopy (TEM) and PL techniques respectively. SEM results showed agglomeration with fluffy shapes having voids and pores and further nanostructural details were obtained with TEM. The divalent europium doped $SrAl_4O_7$ phosphors showed broad band emission spectra at 506 nm due to $^8H_{3/2} \rightarrow {}^8S_{7/2}$ transition on excitation at 360 nm. The prepared nanophosphors had high brightness and long afterglow properties which could be efficiently applied in variety of potential light emitting applications.

1 Introduction

The persistent phosphors are the materials in which phosphorescence is long lasting for several hours at room temperature upon excitation with ultraviolet or natural light source [1–3]. Long lasting phosphors have numerous application, thus have fascinated in current years because of study of their afterglow mechanism [4, 5]. The aluminates and silicates persistent phosphors are the most promising long lasting phosphors due to their advantages of high quantum efficiency, long duration, as well as stable physical and chemical properties [6–8]. The afterglow luminescence is reported from a $SrAl_2O_4:Eu^{2+}$ phosphor at 515 nm which lasts for several minutes [9] and is based on a conventional lattice-defect model this is ascribed to a hole-trapping mechanism [10, 11].

Electronic transition mechanism regulates the luminescence transitions, thus any modification in electronic arrangement of the activator ion due to a change in the size of particle will effect luminescence transitions. The surface states of phosphors are responsible in changing the electronic arrangement of the relaxed excited 5d state of the europium ion. Eu^{2+} doped strontium and aluminum containing double oxides, reveal outstanding long afterglow luminescence and high quantum efficiency properties [11, 12].

$SrAl_4O_7$ is synthesized using a spray-dried [13], solid state [14] and sol–gel precursor route [15–17] at 1050 °C for 2 h heating in a reducing atmosphere. Gel combustion synthesis method has been established to produce crystalline, homogeneous and fine oxide powders, thus is a good alternative to other time-consuming synthetic procedures. In this paper, we applied gel combustion synthesis for the synthesis of Eu^{2+} doped and other RE^{3+} codoped $SrAl_4O_7$ phosphors. The boron flux was used for the preparation of these nanophosphors which helps in the efficient reduction of Eu^{3+} to Eu^{2+} ions. The synthesized phosphors are further characterized by XRD, FTIR, PL, SEM and TEM analysis. The effect of rare earths used as codopants has also been studied.

✉ Devender Singh
devjakhar@gmail.com

[1] Department of Chemistry, Maharshi Dayanand University, Rohtak, Haryana 124001, India

[2] Centro de Fisica, Universidade of Minho, Braga 4710057, Portugal

[3] Departament de Física Aplicada, Universitat Politècnica de València, Valencia 46022, Spain

2 Experimental

2.1 Synthesis

For preparing powdered nanophosphors, highly pure strontium and aluminium metal nitrates, Europium nitrates and urea were weighed in a proper stoichiometric ratio and mixed with some drops of water. Besides these, dysprosium oxide (Dy_2O_3) and neodymium oxide (Nd_2O_3) after converting into nitrates by mixing with concentrated nitric acid were also mixed with previously prepared metal nitrates and urea solution, taken as co-activators. The 5–15 mol% of boric acid (molecular weight for each addition of 0.01 M of Eu^{3+} ion) was also added to the mixture, it was used as flux as well as reducing reagent, while urea [$CO(NH_2)_2$] was used as fuel. The best result was obtained when 12 mol% of boric acid (molecular weight for each addition of 0.01 M of Eu^{3+} ion). This mixed solution was transferred into a silica crucible and the crucible was placed into a furnace set already at 600 °C. Within 5 min, reaction started and caught fire. The mixture formed froths and swelled forming foam, which ruptured with a fire. The process continued for nearly 5 min. After the completion of process, crucible was removed out from the furnace. Upon cooling, fluffy material was obtained (Fig. 1). The synthesis is represented in equation as follows:

$$1 - x\left[Sr(NO_3)_2\right] + 4Al(NO_3)_3.9H_2O + x(Eu(NO_3)_3.6H_2O + 6CO(NH_2)_2 \rightarrow Sr_{1-x}Al_4O_7 : Eu_x^{2+} + 13N_2 + 6CO_2 + 48H_2O$$

2.2 Instrumentation

For the phase confirmation of the as prepared powder, it was characterized by X-ray diffraction patterns of sample using Rigaku Ultima IV X-ray diffractometer with Cu–Ka radiation for $10 \leq \theta \leq 70°$. Morphology of phosphors was studied by using Leo 435 VP scanning electron microscope and a TECNAI 200 kV (Fei, Electron Optics) transmission electron microscope. The compound structural study was done by taking FTIR spectra of samples by using a Nicolet 5700 infrared spectrometer. Optical characterization (emission and excitation spectra) of the materials synthesized was carried out using a Fluorimeter SPEX Fluorolog 1680 (USA) equipped with the SPEX 1934 D phosphorimeter consisting Xenon lamp as excitation source at room temperature in the UV–Visible region.

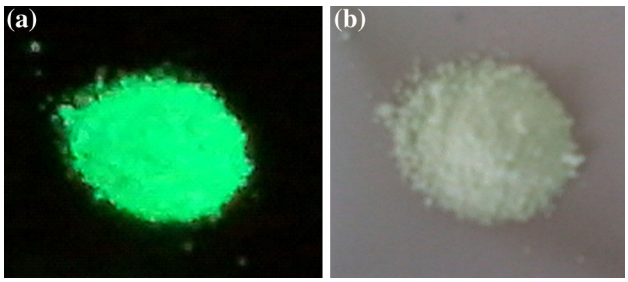

Fig. 1 Nanophosphor material **a** under UV excitation (360 nm), **b** without UV excitation

3 Results and discussions

3.1 X-ray diffraction pattern

X-ray diffraction (XRD) measurements were performed for determining the phase purity, homogeneity and chemical nature of the phosphors. XRD patterns of the series of samples analogous to $SrAl_4O_7$ phosphors, prepared by gel combustion at 600 °C are presented in Fig. 2. The sharpness in diffraction peaks show good crystallinity in prepared phosphor materials. An excellent match is observed for the diffraction peaks of prepared phosphors corresponding to the JCPDS file number 70-1479 which belongs to $SrAl_4O_7$ having monoclinic structure (α-form). The major phase is found $SrAl_4O_7$ from this comparison. Monoclinic α-$SrAl_4O_7$ consist of a three-dimensional $(Al_4O_7)_\infty$ network of AlO_4 units [18, 19].

It is considered that due to having similar ionic sizes the Eu ions (rEu = 1.09 Å) substituted the Sr ions (rSr^{2+}=1.12 Å) in the lattice. Doping in host matrix shows no other effects except variations in intensities. From the XRD pattern shown in Fig. 2, the crystallite sizes were calculated using Scherrer equation.

$$D = k\lambda/\beta\cos\theta$$

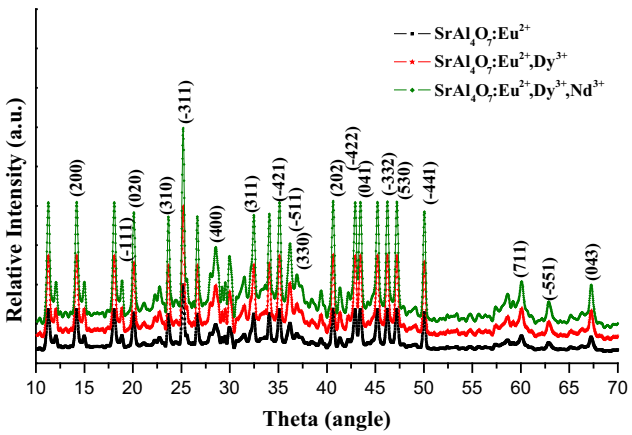

Fig. 2 X-ray diffraction patterns of the synthesized nanophosphors

where k is a constant depending on particle shape, λ is wavelength of X-ray (1.541 Å), β is full width half maxima and θ is Bragg's angle (Table 1).

3.2 FTIR analysis

The FTIR spectra of the series of phosphor samples were taken in the 4000–400 cm^{-1} region and are illustrated in Fig. 3. Both antisymmetric bending (500–650 cm^{-1}) and antisymmetric stretching (720–900 cm^{-1} region) for O–Al–O were obtained in the spectra. The peaks 700–900 cm^{-1} were also attributed to Sr–O bond vibrations. In aluminate phosphors, the lattice structure was constructed of AlO_4 tetrahedral and the structure channels were occupied by Sr^{2+} ions. A symmetric bending in all phosphors in O–Al–O showed two peak at 447 and 420 cm^{-1} (doublet).

3.3 Morphology of synthesized series of phosphor samples

The microstructures of the series of $SrAl_4O_7$ phosphors prepared at 600 °C were analyzed by scanning electron micrographs. The exothermicity generated due to the redox reaction among all the nitrates and fuel, allowed the production of huge amount of gasses and heat. Due to liberation of large amount of gasses the formed powder was voluminous, fine and frothy in each phosphor sample. Samples prepared by gel combustion method showed flakes like morphology with non-uniform distribution (Fig. 4a–c).

Transmission Electron Micrographs (TEM) for the samples indicated highly agglomeration in particles with an average crystal size of ~20–40 nm as shown in Fig. 5a–c. TEM analysis has provided further more micro structural information of these nanophosphors. Most of the particles of the phosphors precursor powders showed irregular shapes with aggregation. Furthermore the crystallite size according to Scherrer's equation is much closer to TEM observation, and it is also confirmed that the obtained phosphors have good crystallinity.

3.4 Photoluminescence properties

Figure 6 shows the emission spectra of Eu^{2+} doped and some trivalent rare earth ions codoped $SrAl_4O_7$

Table 1 Calculated average size for the prepared phosphor crystallites

Phosphor material	2θ value	Particle size (nm)
$Sr_{0.98}Al_4O_7:Eu^{2+}_{0.02}$	25.20	17.86
$Sr_{0.97}Al_4O_7:Eu^{2+}_{0.02},Dy^{3+}_{0.01}$	25.220	23.82
$Sr_{0.96}Al_4O_7:Eu^{2+}_{0.02},Dy^{3+}_{0.01},Nd^{3+}_{0.01}$	24.840	36.08

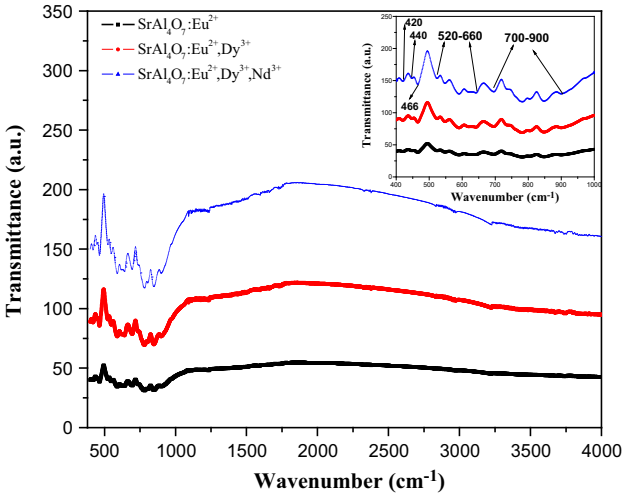

Fig. 3 FTIR spectra of the prepared nanophosphors

nanophosphors. The excitation spectra are also shown in Fig. 6 (inset). These samples on excitation with UV light (λ_{ex} = 360 nm) showed a wide absorption band and then emitted green light. The appearance of green emission indicates that dopant ion europium is available in divalent state. When Dy^{3+} and Nd^{3+} (each 0.01 mol) are used as codopants in the phosphors lattice, then the shape of the excitation and emission spectra remained same, but the excitation and emission intensities are found increased. The broad excitation band is accredited to the transition from state of $4f^7$ configuration to the states $4f^65d^1$ configuration. At room temperature, both the emission and excitation spectra are in the form of broad bands. The excitation spectra show broad band between 290 and 410 nm analogous to the crystal field splitting of d-orbital of the divalent europium ions. Luminescence is found intense due to the allowed transition. Eu^{2+} in $SrAl_4O_7$ showed emission in the green region (~400–600 nm), this is attributed to allowed $^8H_{3/2} \rightarrow {}^8S_{7/2}$ electric dipole transition. Generally crystal field strength and the degree of covalency of europium ions with the surrounding oxygen ions affect the emission of a phosphor. The emissions of phosphors centered at 506 nm (excited at 360 nm). However, no other special excitation and emission lines of trivalent europium were obtained in Fig. 6 which shows that europium is completely reduced to divalent state from trivalent state (gives emission at 613 nm) in the host matrix.

The reduction of Eu^{3+} ions into Eu^{2+} is due to the lattice effect and boric acid (flux) effect. Monoclinic α-$SrAl_4O_7$ consist of a three-dimensional $(Al_4O_7)_\infty$ network of AlO_4 units [18, 19]. AlO_4 units form three dimensional hard tetrahedral anion glass network structures; these possibly protect the Eu^{2+} ions from oxygen to oxidize again in Eu^{3+} in non reducing atmospheric condition [20]. After the addition of boric acid luminescence get much

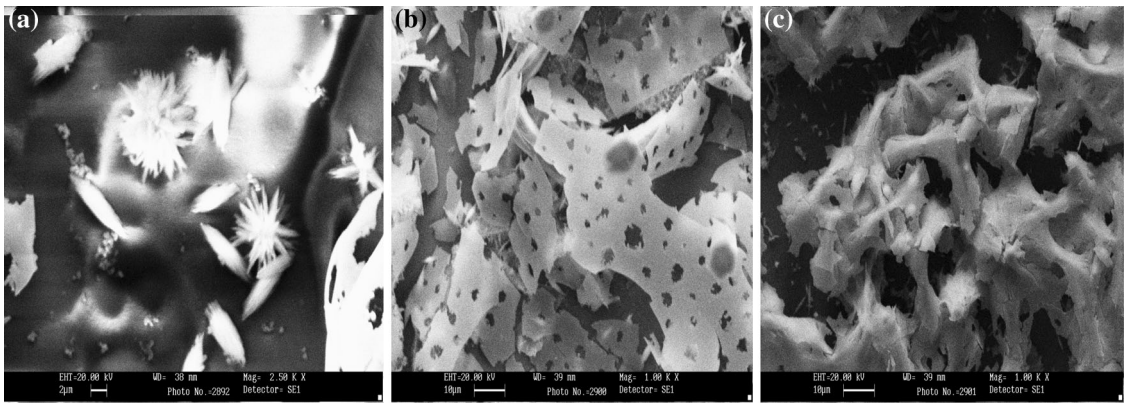

Fig. 4 SEM morphology of: **a** $SrAl_4O_7:Eu^{2+}$, **b** $SrAl_4O_7:Eu^{2+},Dy^{3+}$, **c** $SrAl_4O_7:Eu^{2+},Dy^{3+},Nd^{3+}$ nanophosphors materials

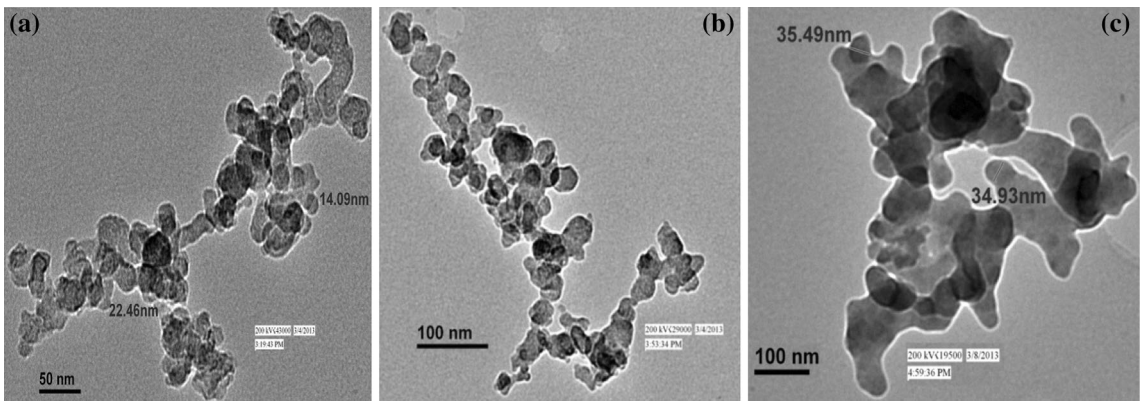

Fig. 5 TEM morphology of: **a** $SrAl_4O_7:Eu^{2+}$, **b** $SrAl_4O_7$: Eu^{2+},Dy^{3+}, **c** $SrAl_4O_7:Eu^{2+},Dy^{3+},Nd^{3+}$ nanophosphors materials

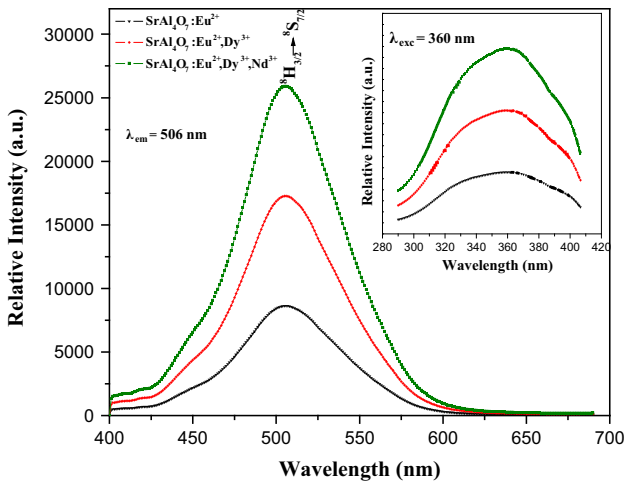

Fig. 6 PL emission and excitation spectrum (*inset*) of $SrAl_4O_7:Eu^{2+},RE^{3+}$ phosphors

enhanced. The reason behind it may be the replacement of Al_2O_3 by B_2O_3 in the host, due to this the tetrahedral borate ions in sample increased steadily, and the tetrahedral aluminate ions decreased. As the ionic size of boron is smaller than that of aluminium so the band strength of B–O is more than that of Al–O band. Consequently, in comparison to tetrahedral aluminate, tetrahedral borate units provide more compactness to the lattice. Resulting there by lattice will shrink on adding boric acid [21]. Therefore, an enhancement in the intensity of emission from Eu^{2+} ions is observed in the emission spectra. Tetrahedral borate anion groups may also be responsible for the reduction of trivalent europium into divalent europium due to probability of transfer of electrons from these groups in non reducing atmospheric conditions [22, 23]. As $[BO_4]$ is having small size than $[AlO_4]$ so electron density is more on borate ions and because of the unstability due to more electron density and small size it is possible to transfer electrons from borate ions to Eu^{3+} ions. One of the other factor is that the Eu^{3+} substitute Sr^{2+} in the host lattice, thus electrons are generated due to charge compensation that reduced the Eu^{3+} ion to its Eu^{2+} form [24]. As boric acid also acts as flux, due to low melting point (460 °C), it provides a medium to facilitate the diffusion of dopant and codopant ions deep across the host matrix [25]. This increases the dopant ions concentration in the strontium aluminate lattice

and causes steep increase in the photoluminescence and also afterglow properties.

Commission Internationale d'Eclairge (CIE) calorimetric coordinates (x, y) can be calculated from the tristimulus value as follows:

$$x = \bar{x}(\lambda)/\bar{x}(\lambda), \bar{y}(\lambda), \text{and}\, \bar{z}(\lambda) \quad (1)$$

$$y = \bar{y}(\lambda)/\bar{x}(\lambda), \bar{y}(\lambda), \text{and}\, \bar{z}(\lambda) \quad (2)$$

The calculated values of color coordinates are shown in Table 2 analogous to green color in visible region on the color triangle (Fig. 7).

3.5 Phosphorescence decay studies

The decay in luminescence of phosphors as shown in Fig. 8 was studied at room-temperature. The curves are showing long decay timing of the prepared phosphors by excitation with long wavelength of UV light for nearly 10 min continuously, e.g. after the switching off excitation source, the emission of light continues from the phosphors for some time.

The decay of the prepared phosphor materials were analyzed by the following second order decay equation [26, 27]:

$$I = I_0 + A_1 \exp(-\tau/\tau_1) + A_2 \exp(-\tau/\tau_2) \quad (3)$$

here, I is the phosphorescence intensity at anytime t after switching off the UV lamp, I_0, A_1, A_2 are the constant and τ_1, τ_2 are decay times for the exponential components of the study of the material.

The phosphorescence in Eu^{2+} (0.02 mol) doped $SrAl_4O_7$ phosphors is thought to arise due to charge carriers i.e., electrons and/or holes, produced on excitation. Charge carriers are trapped at some defect sites, and these are detrapped on thermally excitation [28, 29]. On removal of an excitation source, the trapped holes probably liberated thermally to the valence band and migrated to recombine with excess electrons in metastable state sites leading to the long afterglow of the luminescence of these materials. Trapped holes shows longer lifetime when required thermal energy for detrapping is very high [30]. Consequently, longer decay times can be due to the higher density of deeper trap levels.

The decay average lifetime was calculated from the following equation [31]:

Table 2 Calculated color coordinates of nanophosphors

	Phosphor compounds	Color coordinates
(a)	$Sr_{0.98}Al_4O_7:Eu^{2+}_{0.02}$	x-0.16792, y-0.40491
(b)	$Sr_{0.97}Al_4O_7:Eu^{2+}_{0.02},Dy^{3+}_{0.01}$	x-0.17465, y-0.4429
(c)	$Sr_{0.96}Al_4O_7:Eu^{2+}_{0.02},Dy^{3+}_{0.01},Nd_{0.01}{}^{3+}$	x-0.16287, y-0.5028

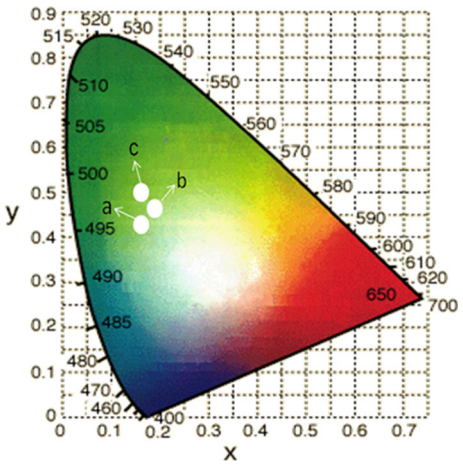

Fig. 7 Chromaticity diagram showing color coordinates

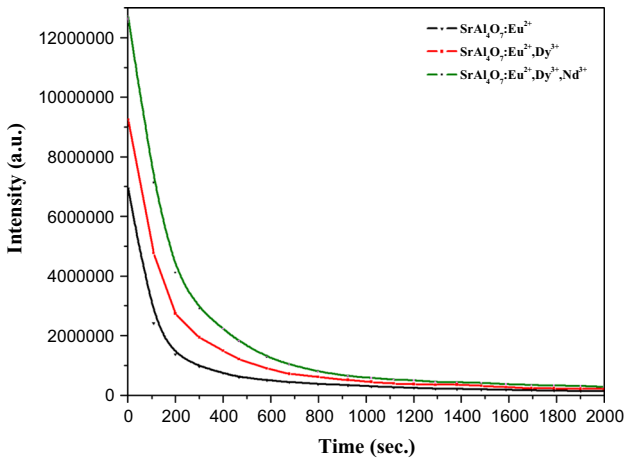

Fig. 8 Decay curve of the prepared nanophosphor materials

$$\tau_{ave} = (A_1\tau_{12} + A_2\tau_{22})/(A_1\tau_1 + A_2\tau_2) \quad (4)$$

All the decay parameters for the phosphors prepared with the present method are given in Table 3.

4 Conclusions

Green light emitting $SrAl_4O_7:Eu^{2+},RE^{3+}$ nanophosphors were synthesized successfully via a rapid gel combustion technique. During the synthesis process, urea not only served as an organic fuel, but also controls the morphology of the nanophosphors. The synthesized phosphors under ultraviolet excitation source exhibited a broad greenish emission at 506 nm associated with the $4f^65d^1 \rightarrow 4f^7$ transition of Eu^{2+} ions. The H_3BO_3 promoted the crystallinity and it properly facilitated the entry of activator ions into the crystal lattice which helped in the formation of luminescent centers (Eu^{2+}). XRD of the crystallites

Table 3 Showing various decay parameters of prepared nanophosphors

Nanophosphor materials	Decay parameters				
	A_1	τ_1 (s)	A_2	τ_2 (s)	τ_{ave} (s)
$Sr_{0.98}Al_4O_7:Eu^{2+}_{0.02}$	156352444	10.72849	2872417.46	338.89866	124.4504661
$Sr_{0.97}Al_4O_7:Eu^{2+}_{0.02},Dy^{3+}_{0.01}$	2878779.312	2.596854	60675.48837	276.87853	194.0245361
$Sr_{0.96}Al_4O_7:Eu^{2+}_{0.02},Dy^{3+}_{0.01},Nd^{3+}_{0.01}$	3368243.948	108.43324	1378786.989	472.67971	341.8639967

show that compound had monoclinic crystalline phase. SEM and TEM techniques explored the formation of the nano-sized crystallites (17–36 nm) of the phosphor. The nano phosphors prepared with rapid gel combustion technique showed high brightness and long after glow properties having their potential applicability in different light emitting technological important fields.

Acknowledgments The authors gratefully recognize the financial support from the University Grant Commission (UGC), New Delhi [MRP-40-73/2011(SR)] and the European Commission through Nano CIS project (FP7-PEOPLE-2010-IRSES ref. 269279).

References

1. Z. Pan, Y.Y. Lu, F. Liu, Nat. Mater. **11**, 58 (2012)
2. K.V. Eeckhout, P.F. Smet, D. Poelman, Materials **3**, 2536 (2010)
3. X.H. Xu, Y.H. Wang, Y. Gong, W. Zeng, Y.Q. Li, Opt. Express **18**, 16989 (2010)
4. A. Bessiere, S. Jacquart, K. Prolkar, A. Lecointre, B. Viana, D. Gourier, Opt. Express **19**, 10131 (2011)
5. Q.M. Chermont, C. Chaneac, J. Seguin, F. Pelle, S. Maitrejean, J.P. Jolivet, D. Gourier, M. Bessodes, D. Scherman, Proc. Natl. Acad. Sci. U.S.A. **104**, 9266 (2007)
6. J. Holsa, H. Jungner, M. Lastusaari, J. Niittykoski, J. Alloys Compd. **323–324**, 326 (2001)
7. W. Zeng, Y.H. Wang, S.C. Han, W.B. Chen, G. Li, Y.Z. Wang, Y. Wen, J. Mater. Chem. C **1**, 3004 (2013)
8. H. Ryu, K.S. Bartwal, J. Alloys Compd. **476**, 379 (2009)
9. C. Chang, D. Mao, J. Shen, C. Feng, J. Alloys. Compd. **348**, 224 (2003)
10. E. Nakazawa, T. Machida, J. Lumin. **72–74**, 236 (1997)
11. V. Abbruscato, J. Electrochem. Soc. **118**, 930 (1971)
12. B. Smets, J. Rutten, G. Hoeks, J. Verlijsdonk, J. Electrochem. Soc. **136**, 2119 (1989)
13. M. Capron, A. Douy, J. Am. Ceram. Soc. **85**, 3036 (2002)
14. X. Yuan, Y. Xu, G. Huang, C. Zeng, J. Am. Ceram. Soc. **90**, 2283 (2007)
15. Y.H. Lin, Z.T. Zhang, F. Zhang, Z.L. Tang, Q.M. Chen, Mater. Chem. Phys. **65**, 103 (2000)
16. P. Escribano, M. Marchal, M.L. Sanjuan, P. Alonso-Gutierrez, B. Julian, E. Cordoncillo, J. Solid State Chem. **178**, 1978 (2005)
17. Y. Liu, C.N. Xu, J. Phys. Chem. B **107**, 3991 (2003)
18. E.R. Boyko, L.G. Wisnyi, Acta Crystallogr. **11**, 444 (1958)
19. A.J. Lindop, D.W. Goodwin, Acta Crystallogr. **B28**, 2625 (1972)
20. C. Zhu, Y. Yang, X. Liang, S. Yuan, G. Chen, J. Am. Ceram. Soc. **90**, 2984 (2007)
21. T.P. Tang, C.M. Lee, F.C. Yen, Ceram. Int. **32**, 665 (2006)
22. Z. Pei, Q. Su, J. Zhang, J. Alloys Compd. **198**, 51 (1993)
23. Q. Zeng, Z. Pei, Q. Su, J. Alloys Compd. **275**, 238 (1998)
24. B. Liu, Y. Wang, J. Zhou, F. Zhang, Z. Wang, J. Appl. Phys. **106**, 053102 (2009)
25. Y.L. Chang, H.I. Hsiang, M.T. Liang, J. Alloys. Compd. **461**, 598 (2008)
26. R. Pang, C. Li, L. Shi, Q. Su, J. Phys. Chem. Solids **70**, 303 (2009)
27. C.H. Huang, T.M. Chen, Opt. Express **18**, 5089 (2010)
28. T. Matsuzawa, Y. Aoki, N. Takeuchi, Y. Murayama, J. Electrochem. Soc. **143**, 2670 (1996)
29. F. Clabau, X. Rocquefelte, S. Jobic, P. Deniard, M.H. Whangbo, A. Garcia, T. Le Mercier, Chem. Mater. **17**, 3904 (2005)
30. G.Y. Lee, W.B. Im, A. Kirakosyan, S.H. Cheong, J.Y. Han, D.Y. Jeon, Opt. Express **21**, 3287 (2013)
31. N. Ruelle, M. Pham-Thi, C. Fouassier, Jpn. J. Appl. Phys. **31**, 2786 (1992)